NASA/TM—2002-211696 AIAA–2002–2419

A Parametric Study of Fine-Scale Turbulence Mixing Noise

Abbas Khavaran
QSS Group, Inc., Cleveland, Ohio

James Bridges
Glenn Research Center, Cleveland, Ohio

Jonathan B. Freund
University of Illinois at Urbana-Champaign, Champaign, Illinois

July 2002

The NASA STI Program Office . . . in Profile

Since its founding, NASA has been dedicated to the advancement of aeronautics and space science. The NASA Scientific and Technical Information (STI) Program Office plays a key part in helping NASA maintain this important role.

The NASA STI Program Office is operated by Langley Research Center, the Lead Center for NASA's scientific and technical information. The NASA STI Program Office provides access to the NASA STI Database, the largest collection of aeronautical and space science STI in the world. The Program Office is also NASA's institutional mechanism for disseminating the results of its research and development activities. These results are published by NASA in the NASA STI Report Series, which includes the following report types:

- TECHNICAL PUBLICATION. Reports of completed research or a major significant phase of research that present the results of NASA programs and include extensive data or theoretical analysis. Includes compilations of significant scientific and technical data and information deemed to be of continuing reference value. NASA's counterpart of peer-reviewed formal professional papers but has less stringent limitations on manuscript length and extent of graphic presentations.

- TECHNICAL MEMORANDUM. Scientific and technical findings that are preliminary or of specialized interest, e.g., quick release reports, working papers, and bibliographies that contain minimal annotation. Does not contain extensive analysis.

- CONTRACTOR REPORT. Scientific and technical findings by NASA-sponsored contractors and grantees.

- CONFERENCE PUBLICATION. Collected papers from scientific and technical conferences, symposia, seminars, or other meetings sponsored or cosponsored by NASA.

- SPECIAL PUBLICATION. Scientific, technical, or historical information from NASA programs, projects, and missions, often concerned with subjects having substantial public interest.

- TECHNICAL TRANSLATION. English-language translations of foreign scientific and technical material pertinent to NASA's mission.

Specialized services that complement the STI Program Office's diverse offerings include creating custom thesauri, building customized data bases, organizing and publishing research results . . . even providing videos.

For more information about the NASA STI Program Office, see the following:

- Access the NASA STI Program Home Page at ***http://www.sti.nasa.gov***

- E-mail your question via the Internet to help@sti.nasa.gov

- Fax your question to the NASA Access Help Desk at 301–621–0134

- Telephone the NASA Access Help Desk at 301–621–0390

- Write to:
  NASA Access Help Desk
  NASA Center for AeroSpace Information
  7121 Standard Drive
  Hanover, MD 21076

NASA/TM—2002-211696 AIAA–2002–2419

A Parametric Study of Fine-Scale Turbulence Mixing Noise

Abbas Khavaran
QSS Group, Inc., Cleveland, Ohio

James Bridges
Glenn Research Center, Cleveland, Ohio

Jonathan B. Freund
University of Illinois at Urbana-Champaign, Champaign, Illinois

Prepared for the
Eighth Aeroacoustics Conference
cosponsored by the American Institute of Aeronautics and Astronautics
and the Confederation of European Aerospace Societies
Breckenridge, Colorado, June 17–19, 2002

National Aeronautics and
Space Administration

Glenn Research Center

July 2002

Acknowledgments

The authors would like to thank Dr. Stewart Leib, NASA Glenn Research Center, for helpful comments in writing the manuscript. In addition, the authors wish to thank Dr. Srini Bhat, Boeing, for providing the jet noise data.

The Aerospace Propulsion and Power Program at
NASA Glenn Research Center sponsored this work.

Available from

NASA Center for Aerospace Information
7121 Standard Drive
Hanover, MD 21076

National Technical Information Service
5285 Port Royal Road
Springfield, VA 22100

Available electronically at http://gltrs.grc.nasa.gov/GLTRS

A PARAMETRIC STUDY OF FINE-SCALE TURBULENCE MIXING NOISE

Abbas Khavaran
QSS Group, Inc.
Cleveland, Ohio

James Bridges
National Aeronautics and Space Administration
Glenn Research Center
Cleveland, Ohio 44135

Jonathan B. Freund
University of Illinois at Urbana-Champaign
Champaign, Illinois 61820

Abstract

The present paper is a study of aerodynamic noise spectra from model functions that describe the source. The study is motivated by the need to improve the spectral shape of the MGBK jet noise prediction methodology at high frequency. The predicted spectral shape usually appears less broadband than measurements and faster decaying at high frequency. Theoretical representation of the source is based on Lilley's equation. Numerical simulations of high-speed subsonic jets as well as some recent turbulence measurements reveal a number of interesting statistical properties of turbulence correlation functions that may have a bearing on radiated noise. These studies indicate that an exponential spatial function may be a more appropriate representation of a two-point correlation compared to its Gaussian counterpart. The effect of source non-compactness on spectral shape is discussed. It is shown that source non-compactness could well be the differentiating factor between the Gaussian and exponential model functions. In particular, the fall-off of the noise spectra at high frequency is studied and it is shown that a non-compact source with an exponential model function results in a broader spectrum and better agreement with data. A recent source model proposed by Tam *et al.* that represents the source as a covariance of the convective derivative of fine-scale turbulence kinetic energy is also examined.

1. Introduction

A physics-based methodology utilizing the averaged equations of motion is used to assess jet noise spectra as a function of the source model function. The focus here is on small-scale turbulence noise that dominates the spectra at subsonic Mach numbers. It is generally accepted that sound generation in jets is a by-product of the unsteady features of the flow. Any flow manipulation intended to reshape the spectra and subsequent perceived noise level ought to affect the unsteady characteristics of the flow.

Mixing enhancement devices such as chevrons and tabs are known to alter turbulence statistics[1] and change the time- and length-scales of noise generating eddies. These flow modifications directly impact the sound field by, for example, reducing the low-frequency noise at the cost of adding to the high-frequency content.

As such, it is not unreasonable to argue that modeling of the unsteady behavior of the flow as supported by a number of isolated test configurations may not lead to a reliable prediction tool. In an ideal situation, one might attempt to solve the full compressible Navier Stokes equations without resorting to any modeling closures. In fact, it is simply a matter of time before Direct Numerical Simulations (DNS) should solve the far-field jet acoustics either directly or by some extension of the near-field solution[2]. Clearly, the computational demands of a typical high Reynolds number jet leave little room, at least in the near future, for DNS as a design code. Nevertheless, it could be an extremely useful tool in understanding the unsteady features of the jet in order to improve the source modeling.

On the other hand, the computational requirements are greatly reduced if the governing equations are spatially filtered, as is done in the Large Eddy Simulation (LES) [e.g., Ref. 3, 4, 5], and the effect of subgrid scales (SGS) is modeled. This approach is successful in capturing the distinct directivity of supersonic jets that results from large scales of motion (instability waves) and dominates the general noise picture near the down-stream axis. But it might also suffer from a neglect of high-frequency noise resulting from subgrid scales. A recent study by Seror *et al.*[6] calculates the acoustic pressure from the filtered Lighthill's stress tensor as well as the full tensor and concludes that the SGS part of the tensor needs to be taken into account in order to recover reliable high-frequency results. One must also be careful about the selection of the subgrid scale eddy viscosity model e.g., constant vs. dynamic Smagorinsky coefficient, as well as the inflow perturbations used in the simulation. LES predictions of Morris *et al.*[3] appear to benefit from the dynamic model and narrow down some of the usual over-predictions in turbulence and noise.

Physics-based prediction methods such as MGBK[7] or Tam and Auriault's[8] fine-scale model heavily rely on model functions that express the statistical properties of noise sources. These predictions use the averaged equations of motion; hence the unsteady features of the flow are entirely described by two-point, space-time correlation models. Any

shortcoming in the predictions should be directly linked to the model. Other phenomena such as refraction and convection impact the directivity of jet noise.

Woodruff *el al.*[9] study the isotropic source model in the original MGBK noise prediction methodology[10] and examine alternative representations for the turbulence spectra. They propose an energy spectrum function for the two-point velocity correlation to satisfy the Kolmogoroff [11] spectrum law in the inertial sub-range. In particular, they examine a wave-number-dependent Gaussian function for the temporal part of the correlation, as opposed to the usual separable space and time functions. Here the characteristic frequency is scaled based on the spatial wave-number k and the turbulence dissipation rate ε as $\tau_o^{-1} \sim k^{2/3}\varepsilon^{1/3}$. The predicted spectra do not appear to offer noticeable improvement over the conventional MGBK methodology that uses a separable correlation function and calculates a characteristic frequency from the turbulence kinetic energy κ as $\tau_o^{-1} \sim \kappa / \varepsilon$. Nonetheless, near 90° angle, they report slight improvement in their spectral shape.

Tam *et al.*[8] model their source as a two-point correlation of the convective derivative of kinetic energy of small-scale turbulence. They use RANS to calculate the time- and length-scales of the noise sources as is done in the MGBK, and predict noise spectra in good agreement with data at mid angles.

In all, the noise from small scales of motion, which are usually broadband in nature and cover a range of observer angles, remains a significant part of the jet noise spectra. Indications are that at high subsonic Mach numbers, and heated jets in particular, instability-associated noise may dominate the low end of the spectra at shallow angles. On the other hand, one might argue that the mean-flow effects could also play a role, by diverting the high-frequency noise of small-scale turbulence away from the axis and creating a region near the zone of silence that is dominated by low-frequency noise.

In this work, alternative representations of the source in modeling the quadrupole terms of Lilley's equation are examined. We concentrate on 90° emission angle where shear-noise is not a factor and the spectral shape is predominantly defined by the self-noise component.

The paper begins with some preliminary formulation of the governing equations. Section 2.2 derives expressions for source and non-compactness factor as a function of the proposed models. It is shown that the fall-off of the high-frequency noise becomes less steep when an exponential spatial function with an appropriate temporal function is selected and non-compactness effects are included. Section 3 compares Tam and Auriault's model[8] with the MGBK model as proposed in Ref [7]. It concludes that the spectral shape at 90° should be identical if consistent assumptions are used. Some concluding remarks on future directions for a physics-based modeling approach is given in the summary.

2. Sound Spectral Density

Application of Lilley's equation to the problem of jet noise and the significance of various source terms has been the subject of numerous discussions in aeroacoustics. In a recent article, Goldstein[12] gives an exact form of the equation with the dependent variable defined such that the source is of quadrupole/dipole nature. The quadrupole source is second-order in velocity fluctuations and is the sum of the commonly known self- and shear noise terms. The dipole term is produced by the fluctuating sound speed due to temperature fluctuations.

The far-field spectral density due to sources of Lilley's equation may be expressed as integration over the source volume $\vec{y}$

$$\overline{p^2}(\vec{x}\,|\,\omega) = \int_{\vec{y}}\int_{\vec{\xi}} G^*(\vec{x},\vec{y}-\vec{\xi}/2,\omega)G(\vec{x},\vec{y}+\vec{\xi}/2,\omega)Q_{12}(\vec{y},\vec{\xi},\omega) \times d\vec{\xi}\,d\vec{y}. \quad (1.1)$$

G is an appropriate Green's function, * denotes a complex conjugate, and Q_{12} is the source spectral density which is formed from a Fourier transform of a two-point space-time correlation between source points $\vec{y}_1 = \vec{y} - \vec{\xi}/2$ and $\vec{y}_2 = \vec{y} + \vec{\xi}/2$ separated by time τ

$$Q_{12}(\vec{y},\vec{\xi},\omega) = \int_{-\infty}^{+\infty} R(\vec{y},\vec{\xi},\tau)e^{i\omega\tau}d\tau\ . \quad (1.2)$$

If we assume that the variation of the magnitude of the Green's function with respect to $\vec{\xi}$, within the source region where Q_{12} is non-zero, is negligible compared to that of its phase then

$$G^*(\vec{x},\vec{y}-\vec{\xi}/2,\omega)G(\vec{x},\vec{y}+\vec{\xi}/2,\omega) \approx |G(\vec{x},\vec{y},\omega)|^2\, e^{-i\vec{k}.\vec{\xi}}, \quad (1.3)$$

where $\vec{k}$ is a wave number of magnitude (ω/a_∞) and direction $(\vec{x}-\vec{y})$. Here ω is the frequency at the observer location and a_∞ denotes the ambient sound speed. Equation (1.1) is now written as

$$\overline{p^2}(\vec{x}\,|\,\omega) = \int_{\vec{y}} |G(\vec{x},\vec{y},\omega)|^2 \int_{-\infty}^{\infty} e^{i\omega\tau}d\tau \int_{\vec{\xi}} R(\vec{y},\vec{\xi},\tau)e^{-i\vec{k}.\vec{\xi}}d\vec{\xi}\,d\vec{y}. \quad (1.4)$$

It is argued that changes in retarded time across a correlation volume element are more likely to be small if the correlation is written in a frame $\vec{x}'$ moving with convection velocity U_c (i.e. $\vec{x}' = \vec{x} - \vec{i}\,U_c t$) of the turbulent eddies. Experimentally, the correlation $R(\vec{y},\vec{\xi},\tau)$ in a jet flow describes a fluctuating pattern in a moving frame and is expressed as

$$R(\vec{y},\vec{\xi},\tau) = R_m(\vec{y},\vec{\xi}_m,\tau), \qquad \vec{\xi}_m = \vec{\xi} - \vec{i}\, U_c\tau. \tag{1.5}$$

Source frequency Ω is related to the observer frequency through the usual Doppler effect $\Omega = \omega(1 - M_c\cos\theta)$. Making a transformation to the moving frame, we find $-\vec{k}.\vec{\xi} + \omega\tau = -\vec{k}.\vec{\xi}_m + \Omega\tau$, therefore

$$\int_{-\infty}^{+\infty} e^{i\omega\tau} d\tau \int_{\xi} R(\vec{y},\vec{\xi},\tau) e^{-i\vec{k}.\vec{\xi}} d\vec{\xi} \equiv \int_{-\infty}^{+\infty} e^{i\Omega\tau} d\tau \int_{\xi_m} R_m(\vec{y},\vec{\xi}_m,\tau) e^{-i\vec{k}.\vec{\xi}_m} d\vec{\xi}_m \tag{1.6}$$

Now the noise spectral density with respect to the moving frame is given as

$$\overline{p^2}(\vec{x}\,|\,\omega) = \int_{\dot{y}} \left| G(\vec{x},\vec{y},\Omega) \right|^2 \int_{-\infty}^{\infty} e^{i\Omega\tau} d\tau \int_{\xi_m} R_m(\vec{y},\vec{\xi}_m,\tau) e^{-i\vec{k}.\vec{\xi}_m} \times d\vec{\xi}_m d\vec{y}. \tag{1.7}$$

2.1 Self Noise Spectra

For brevity, subscript m is suppressed in this section, and $\vec{\xi}$ is used as the separation vector with respect to the moving frame.

To assess the far-field mean-square pressure due to the self-noise term only, we write Lilley's equation in a coordinate $\vec{x}'$ moving with convection velocity U_c

$$L(p_{self};V,x_1') = D\left(\rho \frac{\partial^2(u_i u_j)}{\partial x_i' \partial x_j'}\right). \tag{2.1}$$

Here L is Lilley operator, $V=U-U_c$, and the density ρ has been moved to the right of operator $D = \partial/\partial t + V\partial/\partial x_1'$ assuming that flow is locally parallel and that density fluctuations are small so ρ is the mean density. The Green's function to the above equation for a source of type $D\{e^{-i\Omega t}\delta(\vec{x}' - \vec{x}_o')\}$ is

$$L(S e^{-i\Omega t};V,x_1') = D\{e^{-i\Omega t}\delta(x_1')\delta(\varphi-\varphi_o)\delta(r-r_o)/r\}. \tag{2.2}$$

In the high frequency limit, S is given as

$$S(\vec{x}',\vec{y},\Omega) = \frac{1}{4\pi R}\frac{a_o/a_\infty}{(1-M_c\cos\theta)(1-M_o\cos\theta)}\left(\frac{\zeta_o}{r_o g_o}\right)^{1/2} \times e^{i\Omega R/a_\infty}\exp\{i\frac{\Omega}{a_\infty}[\int_0^\infty (g-g_\infty)dr - \zeta_o\cos(\varphi-\varphi_o)]\} \tag{2.3}$$

where

$$\zeta = \int_0^r g(r,\theta)dr. \tag{2.4}$$

Subscript o refers to source location and the shielding function $g(r,\theta)$ is defined in Appendix A.

The above expression for S is applicable outside the zone of silence of a source only, where the shielding function $g^2(r,\theta)$ is positive at all radial positions; hence there is no shielding. The acoustic pressure due to the above source and Green's function becomes

$$p_{self}(\vec{x}',t) = \int_{-\infty}^{+\infty}\int_{\dot{y}} \hat{S}(\vec{x}',t;\vec{y},t_1)\rho\frac{\partial^2(u_i u_j)}{\partial y_i \partial y_j} dt_1 d\vec{y}, \tag{2.5}$$

$\hat{S}(\vec{x}',t;\vec{y},t_1)$ is the inverse Fourier transform of $S(\vec{x}',\vec{y},\omega)$

$$\hat{S}(\vec{x}',t;\vec{y},t_1) = \frac{1}{2\pi}\int_{-\infty}^{+\infty} S(\vec{x}',\vec{y},\Omega)e^{-i\Omega(t-t_1)}d\Omega \tag{2.6}$$

Upon transferring the derivatives from the source to the Green's function in (2.5), and making the approximation that the variation of the magnitude of the Green's function $S(\vec{x}',\vec{y},\omega)$ with respect to separation vector $\vec{\xi}$ within the source region is negligible compared to that of its phase, we find

$$\overline{p_{self}^2}(\vec{x}|\omega) = \int_{\dot{y}} |S_{,ij}(\vec{x}',\vec{y},\Omega)S_{,kl}(\vec{x}',\vec{y},\Omega)|I_{ijkl}(\vec{y},\Omega)d\vec{y}. \tag{2.7}$$

Subscripts on S refer to derivatives with respect to source coordinate $\vec{y}$, and the phase factor $e^{-i\vec{k}.\vec{\xi}}$ is now included with the source correlation I_{ijkl}. In addition, we have neglected the mean density gradients so that density ρ is included within source correlation function

$$I_{ijkl}(\vec{y},\Omega) = \rho^2\int_{\xi}\int_{-\infty}^{+\infty}\overline{(u_i u_j)(u_k' u_l')}\, e^{-i\vec{k}.\vec{\xi}} e^{i\Omega\tau} d\tau d\vec{\xi}. \tag{2.8}$$

The volume integration in (2.7) usually includes the most energetic parts of the jet. For axisymmetric jets, the directivity factor may be averaged azimuthally with respect to source and observer circumferential angles to obtain a ring-source directivity factor, a_{ijkl}. Subsequently, jet volume integration will be limited to radial and axial coordinates

$$a_{ijkl} \equiv \frac{1}{4\pi^2}\int_{-\pi-\pi}^{+\pi+\pi}\int |S_{,ij}S_{,kl}| d\varphi d\varphi_o, \tag{2.9}$$

$$\overline{p^2}(\vec{x}|\omega) = \int_{-\infty}^{\infty}\int_{0}^{\infty} a_{ijkl} I_{ijk\ell}(\vec{y},\Omega)(2\pi r\, dr dy_1). \tag{2.10}$$

Equation (2.10) is written in an expanded form for a unit ring-source volume at point $\vec{y}$

$$\sum(self\ Noise) = I_{1111}a_{1111} + I_{2222}a_{2222} + I_{3333}a_{3333} + 2I_{1122}a_{1122} + 4I_{1212}a_{1212} + 2I_{1133}a_{1133} + 4I_{1313}a_{1313} + 2I_{2233}a_{2233} + 4I_{2323}a_{2323}, \tag{2.11}$$

Directivity factors a_{ijkl}, and shielding coefficients β_{ij} are defined in Appendix A. In axisymmetric jets,

$$a_{2222} = a_{3333},\ a_{1212} = a_{1313} = a_{1122} = a_{1133},$$
$$a_{2233} = a_{2323}$$

At 90° (2.11) simplifies

$$\sum(Self\ Noise) = 2I_{2222}a_{2222} + 2(I_{2233} + 2I_{2323})a_{2233}, \qquad \theta = 90^{o}. \tag{2.12}$$

At this point, a physics-based modeling approach is employed to obtain closed-form expressions for the correlation coefficients appearing in (2.11) and (2.12). For convenience, we assume that the joint probability distribution of velocities u and u' at points $\vec{y}$ and $\vec{y}'$ (separated in space and time) is normal and write the fourth-order cross-correlation function as a superposition of second-order correlations[13]. In addition, the second-order correlation is assumed separable, i.e., $\overline{u_i u_j'} = R_{ij}(\vec{\xi})\mathcal{G}(\tau)$. Here $R_{ij}(\vec{\xi})$ and $\mathcal{G}(\tau)$ denote the spatial and temporal parts of the correlation, respectively. From (2.8), the axial correlation coefficient becomes

$$I_{1111}(\vec{y},\Omega) = 2\rho^2 \mathrm{G}(\Omega)\int_{\vec{\xi}} R_{11}^2(\vec{\xi})e^{-i\vec{k}\cdot\vec{\xi}}\,d\vec{\xi},$$
$$\mathrm{G}(\Omega) \equiv \int_{-\infty}^{+\infty} \mathcal{G}^2(\tau)e^{i\Omega\tau}d\tau. \tag{2.13}$$

In homogeneous isotropic turbulence, the two-point correlation function has the form[11]

$$R_{ij}(\vec{\xi}) = \overline{u_1^2}[(f + \frac{1}{2}\xi f')\delta_{ij} - \frac{1}{2}f'\xi_i\xi_j/\xi]. \tag{2.14}$$

In the following discussion we examine Gaussian as well as exponential spatial functions $f(\xi)$.

2.2 Compact Eddy Approximation

In a compact eddy approximation, the assumption is made that the eddy length-scale l is much shorter than the wavelength of the acoustic disturbances, i.e. $\omega l / a_\infty$ is small compared to unity. As such the factor $e^{-i\vec{k}\cdot\vec{\xi}}$ is set equal to unity, which practically amounts to setting the wave number equal to zero. Thus the four-dimensional transform (2.8) simplifies.

$$I_{ijkl}(\vec{y},\Omega) \cong \rho^2 \int_{\vec{\xi}}\int_{-\infty}^{+\infty} \overline{(u_i u_j)(u_k' u_l')}\, e^{i\Omega\tau}d\tau d\vec{\xi} \qquad \text{(compact-eddy).} \tag{2.15}$$

Using an appropriate model in (2.13) with $k = 0$ one finds

$$a.\ I_{1111}(\vec{y},\Omega) = \frac{1}{2\sqrt{2}}\rho^2(\overline{u_1^2})^2\ell^3\mathrm{G}(\Omega), \qquad f(\xi) = \exp(-\pi\frac{\xi^2}{\ell^2})$$

$$b.\ I_{1111}(\vec{y},\Omega) = \frac{4}{5\pi^2}\rho^2(\overline{u_1^2})^2\ell^3\mathrm{G}(\Omega), \qquad f(\xi) = \exp(-\pi\frac{\xi}{\ell})$$

$$c.\ I_{1111}(\vec{y},\Omega) = \frac{1}{2\sqrt{2}}\rho^2(\overline{u_1^2})^2\ell_1\ell_2^2\,\mathrm{G}(\Omega),\ \Gamma(\vec{\xi}) = \exp\{-\pi(\frac{\xi_1^2}{\ell_1^2} + \frac{\xi_{23}^2}{\ell_2^2})\}$$

$$d.\ I_{1111}(\vec{y},\Omega) = \frac{4}{5\pi^2}\rho^2(\overline{u_1^2})^2\ell_1\ell_2^2\,\mathrm{G}(\Omega),\ \Gamma(\vec{\xi}) = \exp\{-\pi\sqrt{\frac{\xi_1^2}{\ell_1^2} + \frac{\xi_{23}^2}{\ell_2^2}}\} \tag{2.16}$$

with $\xi_{23}^2 = \xi_2^2 + \xi_3^2$. Models (a) and (b) assume isotropic turbulence, whereas (c) and (d) use an axisymmetric turbulence constructed from a set of kinematically compatible scalar functions [Ref .7]. Length-scales ℓ_1 and ℓ_2 are proportional to $(\overline{u_1^2})^{3/2}/\varepsilon$ and $(\overline{u_2^2})^{3/2}/\varepsilon$, respectively.

Consider the isotropic model, cases (a) and (b). After substituting the remaining correlation coefficients into (2.12) (see Appendix B) we find

$$\sum(Self\ Noise) = 2(a_{2222} + a_{2233})I_{1111}. \qquad \theta = 90^{o} \tag{2.17}$$

The shielding coefficients β_{ij} that multiply directivity factor a_{ijkl} result in noise attenuation within the zone of silence. At 90° emission angle, $\Omega = \omega$, and the shielding function is $g^2(r) = (a_\infty / a)^4$, where a is the sound speed at the source. Here $g^2(r)$ has no zero crossing, therefore there is no turning point and $\beta_{ij} = 1$.

$$\sum(Self\ Noise) = |S|^2 k^4 (\frac{a_\infty}{a})^4 I_{1111}, \qquad \theta = 90^{o} \tag{2.18}$$

Away from 90° equation (2.11) should be used directly. In addition, the shear noise contribution needs to be included as described in Ref [7]. Model (c) shows that the directivity of jet noise with respect to its level at 90° is a function of anisotropy of turbulence[7].

Let τ_o be the inverse of the characteristic source frequency, which is proportional to turbulence kinetic energy and its dissipation rate as $\tau_o^{-1} = \Omega_o = \alpha_1 \varepsilon / \kappa$. Eddy length-scale is obtained from $\ell \sim \tau_o u_1$. At this point noise spectrum at 90° may be calculated using models (a) or (b) in (2.18) and with an appropriately selected proportionality factor for ℓ. It is clear that the spectral shape will be the same for both models. For instance, if the proportionality factor selected for length-scale ℓ in model (b) was larger than that of model (a), say by factor $(5\pi^2 / 8\sqrt{2})^{1/3}$, then identical spectra are obtained.

Upon examining the three-dimensional energy spectrum for a two-point correlation $R_{ij}(\vec{\xi})$ using models (a) and (b), it is found that both scale as fourth power of spatial wave number when wavelength is large. However, in the inertial sub-range, their decay rate is substantially different. The energy spectrum function, normalized with respect to $(1.5\,\overline{u_1^2})$, is given as

$$E(k) = \frac{\ell}{12\pi}\frac{(k\ell)^4}{(4\pi)^2}\exp(-\frac{k^2\ell^2}{4\pi}), \qquad f(\xi) = \exp(-\pi\frac{\xi^2}{\ell^2})$$

$$E(k) = \frac{16\ell}{3\pi^2}\frac{(k\ell/\pi)^4}{(1+\frac{k^2\ell^2}{\pi^2})^3}, \qquad f(\xi) = \exp(-\pi\frac{\xi}{\ell}). \tag{2.19}$$

Figure 1 shows that the energy spectrum for the exponential function (model b) decays as k^{-2} at large spatial wave number. This is reasonably close to the proposed Kolmogoroff's $k^{-5/3}$ scaling law[11]. Model (a), however, presents a much faster decay rate. These comparisons suggest that when non-compactness effects are accounted for, the two models, if properly used, should produce different spectral decay at high frequency (this will be shown in section 2.4).

Reference [11] argues that the exponential function may not be strictly correct on the grounds that (1) it is not parabolic at its vertex, (2) the lateral correlation $\overline{u_1 u_1}$ with $\vec{\xi}$ in direction of ξ_2 remains positive for all ξ_2; whereas the correct curve must become negative for large ξ_2.

Recent measurements of Bridges *et al.*[14] appear to suggest that a two-point correlation $R_{ij}(\vec{\xi})$ constructed from an exponential spatial function according to (2.14) provides a better fit to data relative to the Gaussian function (Fig. 2).

2.3 Source Non-Compactness

Here we explore the effect of source non-compactness on noise spectra using Gaussian and exponential models (a) and (b). To carry out the integration with respect to $\vec{\xi}$ in (2.8) or (2.13), a convenient coordinate transformation has one of the axes ξ_i aligned with vector $\vec{k}$.

In a spherical coordinate $\vec{\xi} = \xi(\cos\alpha,\ \sin\alpha\cos\varphi,\ \sin\alpha\sin\varphi)$, ξ_1 is aligned with wave number $\vec{k}$ such that $\vec{k}.\vec{\xi} = k\xi\cos\alpha$. Equivalently, one might select a cylindrical coordinate system $\vec{\xi} = (\xi_1,\ r\cos\varphi,\ r\sin\varphi)$ with ξ_1 in the direction of $\vec{k}$ such that $\vec{k}.\vec{\xi} = k\xi_1$. In any event, when turbulence is isotropic, the final result should be independent of the direction of wave number $\vec{k}$. Now with $f(\xi) = \exp(-\pi\xi^2/\ell^2)$ we find

$$I_{1111}(\vec{y},\Omega) = \frac{1}{2\sqrt{2}}\rho^2(\overline{u_1^2})^2\ell^3\mathrm{G}(\Omega)N(k\ell),\ N(k\ell) = \exp(-\frac{k^2\ell^2}{8\pi}) \tag{2.20}$$

where $N(k\ell)$ denotes the non-compactness factor. Using an exponential function $f(\xi) = \exp(-\pi\xi/\ell)$ we find

$$I_{1111}(\vec{y},\Omega) = \frac{4}{5\pi^2}\rho^2(\overline{u_1^2})^2\ell^3\mathrm{G}(\Omega)N(k\ell),$$

$$N(k\ell) = 20(\frac{\pi}{k\ell})^5\,[\,3\tan^{-1}(\frac{k\ell}{2\pi}) - 2\frac{k\ell}{\pi}\frac{5(\frac{k\ell}{\pi})^2+12}{\left((\frac{k\ell}{\pi})^2+4\right)^2}\,]. \tag{2.21}$$

Applying the law of limits repeatedly, the last expression for $N(k\ell)$ becomes 1 as $k\ell$ approaches zero. Figure 3 shows that the non-compactness factors equal 1.0 for $0 \le k\ell < 2$ and decay rapidly for $k\ell > 7$. The Gaussian function appears to produce a faster-decaying non-compactness factor. The above non-compactness factors repeat for other correlation coefficients as noted in Appendix B.

Since $\ell \sim \tau_o u_1$, we find $k\ell \sim (\omega\tau_o)(u_1/a_\infty)$. Ratio u_1/a_∞ is usually smaller than 1.0 (of the order of 0.2 for the more energetic parts of the jet). In the compact eddy approximation $k\ell$ was assumed small hence $N(k\ell)$ was set equal to 1.0 for the entire range of the wave number. As frequency ω becomes very large, $\omega\tau_o$ may be large enough to reduce N below 1.0 (Fig. 3).

The implications are that the effect of $N(k\ell)$ on spectra, if any, should be a slower decay rate at high frequency for the exponential function relative to the Gaussian. It is also evident that both models produce a faster decay at high frequency when the sources become non-compact. However,

as we shall see shortly, these effects are visible only in the context of the spectral shape function $G(\Omega)N(k\ell)$. If $G(\Omega)$ has already decayed far enough before $N(k\ell)$ takes effect, then both models produce identical spectra.

Figure 4 shows the MGBK prediction using Gaussian-isotropic source model (a). The effect of source non-compactness on predicted noise spectra for a Mach 0.5 cold jet is of the order of 0.12 dB at the high end of the spectra. Here the temporal part of the correlation was selected as[7]

$$g(\tau) = \exp\{-\sqrt{(\sigma/2)^2 + (\tau/\tau_o)^2}\}. \qquad (2.22)$$

Constant σ = 0.8 as was originally proposed in Ref [7]. One might expect a similar effect at other angles, as $N(k\ell)$ is a common factor throughout Eq. (2.11).

Next we explore the MGBK spectral shape function.

2.4 Spectral Shape Function

Apart from factor k^4, which appears due to transfer of derivatives from source to the Green's function (not included in the following discussion), the spectral shape function, denoted as $\hat{F}_1(\omega\tau_o)$, is simply the product $G(\Omega)N(k\ell)$. Function $G(\Omega)$ is obtained from (2.13) and (2.22)

$$\hat{F}_1(\omega\tau_o) = \sigma\tau_o \frac{K_1[\sigma\sqrt{1+(\Omega\tau_o/2)^2}]}{\sqrt{1+(\Omega\tau_o/2)^2}}\ N(k\ell) \qquad (2.23)$$

The normalized spectral function becomes

$$\hat{F}_1(\omega\tau_o) = \frac{K_1[\sigma\sqrt{1+(\Omega\tau_o/2)^2}]}{\sqrt{1+(\Omega\tau_o/2)^2}\ K_1(\sigma)}\ N(k\ell), \qquad (2.24)$$

$$\Omega = \omega(1 - M_c\cos\theta).$$

As σ becomes very small one finds

$$\lim_{\sigma\to 0} \hat{F}_1 = \frac{1}{1+(\Omega\tau_o/2)^2} N(k\ell) \qquad . \qquad (2.25)$$

Figure 5 shows the spectral shape function $\hat{F}_1(\omega\tau_o)$ for model (a), with $\ell/(U\tau_o) = 0.20$, which applies to the more energetic parts of the flow. Fig 5a shows a negligible role for the non-compactness factor at $\sigma = 0.80$. The effect of $N(k\ell)$ becomes evident as shown in Figures 5b and 5c. It should be noted that when $\sigma \to 0$ the compact source model becomes increasingly inadequate (resulting in unusually high level of noise at high frequency).

Comparison of the spectral shape functions of models (a) and (b) shows a slower high- frequency decay for the exponential model (Figs. 6a and 6b). Shown in Fig. 7 is the MGBK predicted spectrum for Mach 0.5 cold jet with $\sigma = 0$, including the non-compactness. Model (b) predicts a broader spectrum and noticeable high-frequency improvement relative to model (a). Here, the location of the peak frequency was adjusted slightly by selecting proportionality constant α_1, ($\tau_o^{-1} = \alpha_1 \varepsilon/\kappa$) as 0.225 and 0.170 for models (a) and (b) respectively.

3. Tam and Auriault's Model

In reference [8], Tam *et al.* compute the fine-scale turbulence noise from an equation similar to (1.4). Here we compare the Green's function as well as the source cross correlation functions between the MGBK model and Tam's approach.

3.1 Green's Function

The Green's function to the linearized Euler equations for a locally parallel flow is the solution to

$$L(Ge^{-i\omega t}; U, x_1) = e^{-i\omega t}\delta(\vec{x} - \vec{x}_s)\ , \qquad (3.1)$$

where ω denotes source frequency with respect to stationary frame $\vec{x}$, $\vec{x}_s$ is the source location, and L is Lilley's operator. Tam and Auriault [15] recast the problem into an adjoint operator for the adjoint Green's function G_a, which is related to the Green's function G of the original problem by a simple switch of the source and observer locations $\vec{x}_s$ and $\vec{x}_o$. The final result for an axisymmetric mean flow (now multiplied by $2\pi a_\infty^2$ to compare with the high-frequency solution) is given as

$$G(\vec{x}_o, \vec{x}_s, \omega) = G_a(\vec{x}_s, \vec{x}_o, \omega)$$

$$G_a(\vec{x}_s, \vec{x}_o, \omega) = \frac{e^{-ik(x\cos\theta - R)}}{4\pi k\, a_\infty R}\sum_{m=0}^{\infty} f_m(r)\cos m\varphi\ , \quad r_s \le R_o\ . \qquad (3.2)$$

Function $f_m(r)$ is obtained by solving an ordinary differential equation and matching the above inner solution with the outer solution at the jet boundary R_o.

$$G_a(\vec{x}, \vec{x}_o, \omega) = \frac{e^{-ik(x\cos\theta - R)}}{4\pi k a_\infty R}\sum_{m=0}^{\infty}[(-i)^m \varepsilon_m J_m(\chi) + A_m H_m^{(1)}(\chi)] \times\cos m\varphi, \quad r \ge R_o \qquad (3.3)$$

where $\chi = kR_o\sin\theta$.

The corresponding high-frequency solution[16] for a non-convecting ($\Omega = \omega$) monopole type source takes one of the following forms depending on the location of the source r_o relative to the zero crossing point r_σ of the shielding function, i.e. $g(r_\sigma) = 0$ (see Appendix A for the definition of g).

$$G(\vec{x},\vec{y},\omega)=\frac{i}{4\pi a_\infty kR}\frac{a_o/a_\infty}{(1-M_o\cos\theta)^2}\left(\frac{\zeta_o}{r_o h_o}\right)^{1/2}e^{ikR}$$
$$\times\exp(ik[\int_{r_\sigma}^{\infty}(g-g_\infty)dr-g_\infty r_\sigma]-k[\zeta_\sigma-\zeta_o\cos(\varphi-\varphi_o)]),\quad r_o<r_\sigma \tag{3.4}$$

with $h^2=-g^2$, $\zeta=\int_0^r h(r,\theta)dr$

or

$$G(\vec{x},\vec{y},\omega)=\frac{i}{4\pi a_\infty kR}\frac{a_o/a_\infty}{(1-M_o\cos\theta)^2}\left(\frac{\zeta_o}{r_o g_o}\right)^{1/2}e^{ikR}$$
$$\times\exp(ik[\int_0^{\infty}(g-g_\infty)dr-\zeta_o\cos(\varphi-\varphi_o)]),\quad r_o>r_\sigma \tag{3.5}$$

with $\zeta=\int_0^r g(r,\theta)dr$.

Figure 8 shows comparisons of the above Green's functions for a stationary ring source at 7 diameters from the jet exit ($x/D=7$), and with radius r_o/D indicated as a parameter. Computations were carried out for a range of Strouhal numbers ($St=fD/U_j$) for a Mach 0.9 cold jet. The agreement is generally good at high frequency. As the Strouhal number is lowered, the high- frequency approximation appears to deteriorate. Discrepancies become increasingly visible near the boundary of zone of silence as seen in figure 8c, with the adjoint Green's function predicting a larger zone of silence. For our purpose, we intend to compare the MGBK spectrum with Tam's solution at $\theta=90^o$ and assess the high-frequency behavior. Spectral peak for both Mach 0.5 and 0.9 cold jets is near St = 0.9, therefore the high-frequency solution is found suitable.

It is noted that the Green's function for a monopole type source scales as k^{-1} with respect to the wave number and as $1/(1-M_o\cos\theta)^2$ with respect to polar angle.

3.2 Source Model

Tam and Auriault[8] propose a two-point, fourth-order, axial velocity correlation in a fixed reference frame

$$\left\langle\frac{Dq_s(\vec{x}_1,t_1)}{Dt_1}\frac{Dq_s(\vec{x}_2,t_2)}{Dt_2}\right\rangle=\frac{\hat{q}_s^2}{c^2\tau_s^2}\exp\{\frac{-|\xi_1|}{U\tau_s}$$
$$-\frac{\ell n\,2}{\ell_s^2}[(\xi_1-U\tau)^2+\xi_{23}^2]\} \tag{3.6}$$

with $\vec{\xi}=\vec{x}_1-\vec{x}_2$, $\tau=t_1-t_2$, ξ_{23} as defined earlier, and U the mean velocity at the source location, which can be replaced with the source convection velocity. In this section we use $\vec{\xi}$ as separation vector in a fixed reference frame.

The corresponding axial correlation coefficient used in the MGBK describes the cross correlation of the Reynolds stress components rather than their convective derivatives. Following the usual MGBK methodology, the fourth-order correlation $I_{1111}(\xi,\tau)=\left\langle(\rho u_1 u_1)(\rho u_1' u_1')\right\rangle$ is expressed as a sum of second-order tensors. The element of I_{1111} contributing to the noise field is simply $2R_{11}^2(\vec{\xi})\mathcal{g}^2(\tau)$ which, upon using model (a) in (2.14), and making a transition to a fixed reference frame, becomes

$$I_{1111}(\vec{\xi},\tau)=2\rho^2\overline{(u_1^2)}^2(1-\frac{\pi}{\ell^2}\xi_{23}^2)^2\exp\{-2\frac{\pi}{\ell^2}[(\xi_1-U\tau)^2$$
$$+\xi_{23}^2]\}\mathcal{g}^2(\tau) \tag{3.7}$$

and temporal function is given by (2.22).

Factor $(1-\pi\xi_{23}^2/\ell^2)$ in (3.7) reduces $I_{1111}(\bar{\xi},\tau)$ to zero as the normalized lateral distance (ξ_{23}/ℓ) approaches $1/\sqrt{\pi}$. Beyond this point the correlation is practically zero.

In order to compare correlation functions (3. 6) and (3.7) on an equal basis, suppose we relate time- and length scales and define the following dimensionless parameters

$$\ell=(\frac{2\pi}{\ell n\,2})^{0.5}\ell_s,\quad \tau_o=2\tau_s,\quad \bar{\xi}_i=\xi_i/\ell_s,\quad \bar{\tau}=\tau/\tau_s. \tag{3.8}$$

Now the lateral correlations, with zero time-delay, and normalized in magnitude become

$$\left\langle\frac{Dq_s(x,t_1)}{Dt_1}\frac{Dq_s(x+\xi_{23},t_1)}{Dt_1}\right\rangle=\exp\{-\ell n\,2\ \bar{\xi}_{23}^2\} \tag{3.9}$$

and

$$I_{1111}(\xi_{23},0)=(1-\frac{\ell n\,2}{2}\bar{\xi}_{23}^{\,2})^2\exp\{-\ell n\,2\,\bar{\xi}_{23}^2\}. \tag{3.10}$$

Figure 9a shows that (3.9) and (3.10) decay somewhat differently. Tam and Auriault's correlation (3.9) does not have a zero intersect and decays at a slower rate. Limited data available on fourth-order correlation measurements[17] seem in better agreement with the MGBK model. However, this difference may practically be insignificant in noise prediction. An interested reader may find more information on the second-order lateral correlation in a book by Townsend[18].

Aside from ξ_{23}, which is now set equal to 0.0, the two models appear similar. The normalized axial cross correlation functions are:

$$\left\langle \frac{Dq_s(x,t_1)}{Dt_1}\frac{Dq_s(x+\xi_1,t_2)}{Dt_2}\right\rangle = \exp\{-\alpha|\overline{\xi}_1| - \ell n\,2\,(\overline{\xi}_1 - \overline{\tau}/\alpha)^2\}, \quad (3.11)$$

$$I_{1111}(\xi_1,\tau) = \exp\left\{-\sqrt{\sigma^2+\overline{\tau}^2} - \ell n\,2\,(\overline{\xi}_1 - \overline{\tau}/\alpha)^2\right\} \quad (3.12)$$

with $\alpha = (\ell_s / U\tau_s)$.

Using Tam's constants ($\ell_s = c_\ell \kappa^{3/2}/\varepsilon$, $\tau_s = c_\tau \kappa/\varepsilon$, $c_\ell = 0.256$, $c_\tau = 0.233$) one finds $\alpha = (c_\ell / c_\tau)(\kappa^{0.5}/U)$. Let's set U equal to the convection velocity $0.65U_J$. In the more energetic parts of the flow (mixing layer) we chose $(\kappa^{0.5}/U_J) \cong 0.12$, and find $\alpha \cong 0.20$.

Figure 9b shows Tam's correlation coefficient (3.11) and the MGBK model (3.12), with $\sigma = 0$. The effect of small parameter σ is shown in figure 9c. Aside from the slight difference described above in comparing the lateral correlations, the two models exhibit similar features.

Next, the spectral shape functions are compared.

3.3. Spectral Function

The MGBK spectral function was written earlier in a moving frame as a Fourier transform of the temporal function $g^2(\tau)$, multiplied by the non-compactness factor. In a fixed frame variable τ appears in $(\xi_1 - U\tau)$, hence the spatial function needs to be include in the integration. However, with a simple transformation $\vec{\xi}_m = \vec{\xi} - U\tau$ (see 1.6), the spectral shape function (2.24) is recovered. For comparison with Tam's spectra we now let $\tau_o = 2\tau_s$ and relate ℓ to ℓ_s (see 3.8).

$$\hat{F}_1(\omega\tau_s) = \frac{K_1[\sigma\sqrt{1+(\Omega\tau_s)^2}]}{\sqrt{1+(\Omega\tau_s)^2}\,K_1(\sigma)}N(k\ell), \quad (3.13)$$

$\Omega = \omega(1 - M_C\cos\theta)$.

$N(k\ell)$ for model (a) is given in (2.20). As σ become small one finds

$$\lim_{\sigma\to 0}\hat{F}_1 = \frac{1}{1+(\Omega\tau_s)^2}N(k\ell). \quad (3.14)$$

Following Eq. 33 [Ref. 8], Tam and Auriault's spectral function $\hat{F}_2$, is written for a unit volume of turbulence at $\vec{y}$

$$\hat{F}_2(\omega\tau_s) = \int_\xi\int_\tau p_a(\vec{y},\vec{x},-\omega)p_a(\vec{y}+\vec{\xi},\vec{x},+\omega)\,d\vec{\xi}\exp\{-\frac{|\xi_1|}{U\tau_s} - \frac{\ell n2}{\ell_s^2}[(\xi_1 - U\tau)^2 + \xi_{23}^2] + i\omega\tau\}d\tau\,d\vec{\xi}. \quad (3.15)$$

Here p_a is the direct Green's function, which is obtained from switching source and observer locations in the adjoint problem. As was done earlier, the product of the Green's functions is approximated as the magnitude at the center of the correlation volume multiplied by a proper phase

$$p_a(\vec{y},\vec{x},-\omega)p_a(\vec{y}+\vec{\xi},\vec{x},+\omega) \approx |p_a(\vec{y},\vec{x},-\omega)|^2 e^{i\vec{k}.\vec{\xi}}. \quad (3.16)$$

Phase factor $\vec{k}.\vec{\xi}$ should not carry a preferred direction since rays are emitted at all angles and separation vector $\vec{\xi}$ may also take any direction. It follows

$$\hat{F}_2(\omega\tau_s) = |p_a(\vec{y},\vec{x},-\omega)|^2 \int_{\vec{\xi}}\int_\tau \exp\{-\frac{|\xi_1|}{U\tau_s} - \frac{\ell n2}{\ell_s^2}[(\xi_1 - U\tau)^2 + \xi_{23}^2] + i\vec{k}.\vec{\xi} + i\omega\tau\}d\tau\,d\vec{\xi},$$

or upon integrating over τ

$$\hat{F}_2(\omega\tau_s) = |p_a(\vec{y},\vec{x},-\omega)|^2 \exp\left(-\frac{1}{\ell n\,2}(\frac{\omega\ell_s}{2U})^2\right)\int_{\vec{\xi}}\exp\{-\frac{|\xi_1|}{U\tau_s} - \frac{\ell n2}{\ell_s^2}\xi_{23}^2 - i\frac{\omega\xi_1}{U} + i\vec{k}.\vec{\xi}\}d\vec{\xi}.$$

As before, make a coordinate transformation with respect to dummy variable $\vec{\xi}$ such that ξ_1 aligns with $\vec{k}$ (i.e. $\vec{k}.\vec{\xi} = k\xi_1$). The component of U in direction of $\vec{k}$ becomes $U_\theta = U\cos\theta$.

$$\hat{F}_2(\omega\tau_s) = |p_a(\vec{y},\vec{x},-\omega)|^2 2\ell_s^3 \exp\left(-\frac{1}{\ell n\,2}(\frac{\omega\ell_s}{2U})^2\right)\int_{-\infty}^{+\infty}\int_{-\infty}^{+\infty}d\xi_2 d\xi_3 \times\int_0^\infty \exp\{-\frac{\ell_s\xi_1}{U_\theta\tau_s} - \ell n2\,\xi_{23}^2\}\cos[(\frac{\omega}{U_\theta} - k)\xi_1]d\xi_1.$$

Next transition to polar coordinates $\vec{\xi} = (\xi_1,\ r\cos\varphi,\ r\sin\varphi)$

$$\hat{F}_2(\omega\tau_s) = |p_a(\vec{y},\vec{x},-\omega)|^2 \frac{2\pi\ell_s^3}{\ell n\,2}\frac{U\tau_s/\ell_s}{1+(\omega\tau_s - U_\theta\tau_s k)^2} \times\exp\left(-\frac{1}{\ell n\,2}(\frac{\omega\ell_s}{2U})^2\right). \quad (3.17)$$

Expression (3.17) is now normalized to obtain the spectral shape function. We also take out the magnitude of the Green's from the spectral function (as was done in 3.13). For a compact eddy ($k = 0$)

$$\hat{F}_2(\omega\tau_s) = \frac{1}{1+(\omega\tau_s)^2}\exp\left(-\frac{1}{\ell n\, 2}\left(\frac{\omega\ell_s}{2U}\right)^2\right), \quad \text{(compact eddy)} \qquad (3.18)$$

and

$$\hat{F}_2(\omega\tau_s) = \frac{1}{1+(\omega\tau_s)^2\left(1-\frac{U}{a_\infty}\cos\theta\right)^2}\exp\left(-\frac{1}{\ell n\, 2}\left(\frac{\omega\ell_s}{2U}\right)^2\right), \quad \text{(non-compact eddy).} \qquad (3.19)$$

This result is the same as that reported by Tam and Auriault, but was derived without resorting to the following approximation, which was suggested in Ref. [8].

$$p_a(\vec{y},\vec{x},-\omega)p_a(\vec{y}+\vec{\xi},\vec{x},+\omega) \cong \left|p_a(\vec{y},\vec{x},-\omega)\right|^2\exp\{ik\xi_1\cos\theta\}$$

At this point let's compare (3.19) with the MGBK shape function (model a) at 90° emission angle. Figure 10 shows comparisons with $\ell_s / U\tau_s$ = 0.20 as was selected earlier. The MGBK spectral shape (with $\sigma = 0.20$) agrees quite favorably with Tam's results at $U/a_\infty = 0.325$ and 0.65 as shown in figure 10a and 10b, corresponding to jet exit velocity of $U_J/a_\infty = 0.50$ and $U_J/a_\infty = 1.0$ respectively.

It is noted that in comparing the above spectral shape functions, we have deliberately dropped the wave number power k^4 from MGBK model (see 2.18), and k^2 from Tam's model. In the MGBK approach, factor k^4 appears when two spatial derivatives and one convective derivative are transferred from source to the Green's function. Tam and Auriault, on the other hand, maintain that convective derivative is included in their source modeling. As a result the Green's function p_a remains of the order of k (see equation (28) of Ref [15]), which incidentally indicates that source q_s should be of quadrupole type. With the convective derivative now hidden in the source, the power spectral function becomes proportional to k^2.

Morris and Farassat[19] described this in more detail in a recent paper and suggested that a consistent approach should result in $\sim k^4$ for both MGBK and Tam's analysis.

Figure 11 shows the MGBK predictions for Mach 0.5 cold jet using model (a) and a spectral shape function that matches that of Tam and Auriault's (curve 1). Predictions obtained by replacing the k^4 wave-number factor by k^2 (as in Tam and Auriault approach) are also shown. In doing so, some minor adjustments had to be made in the calibration constant related to the source characteristic frequency to persevere the location of the peak spectra. The noise spectrum naturally becomes broader with the k^2 factor (compare 1 and 2), and improvements are noticed at both ends.

Additional high-frequency improvement could be gained by simply removing the atmospheric attenuation built in the MGBK code from predictions and implying that it is built into the source model (as was done in spectral predictions of Ref. 8 at *R/D* = 100). However, predicted noise spectrum should account for atmospheric attenuation. This amounts to attenuating the high-frequency noise depending on the observer distance and atmospheric conditions (i.e., relative humidity and ambient temperature). Noise measurements usually reflect the atmospheric attenuation. Figure 11 (curve 3) shows the significance of atmospheric loss on predicted spectra. Although excellent agreement with data is thereby obtained, two very questionable steps were taken to predict a better spectrum.

As was shown earlier (Fig. 7), good agreement with data could be achieved by selecting an exponential spatial function (model b) in place of the Gaussian function.

4. Concluding Remarks

In the preceding discussions, we examined alternative model representations for the two-point space-time correlation appearing in physics-based jet noise prediction methodologies. It was argued that a proper representation of the source, consistent with the observations and accepted fundamentals related to turbulence statistics, should improve prediction of the flow-generated noise in the framework of Lilley's equation. The discussions centered on noise from small-scales of motion and at 90° observer-angle. The main result of the study was described in Fig. 7. It was shown that an exponential spatial function, with source non-compactness included, predicts a broader spectrum relative to a Gaussian function. The effect of turbulence anisotropy may readily be accounted for by selecting model (d) of section 2.2 as a non-compact source.

Away from 90°, mean-flow refraction effects as well as convective amplification due to source motion become crucial in capturing the peak directivity that occurs near the down-stream axis. A high-frequency approximation offers an analytical solution to the Green's function, but comparisons of section 3.1 indicate that it might not be an appropriate approximation at small Strouhal numbers.

A numerically computed Green's function[15] provides extra flexibility at low frequency, at the cost of added numerical intensity.

Appendix A

Directivity factor for various quadrupole source components (in the absence of mean density gradient) is

$$a_{1111} = \frac{\cos^4\theta}{(1-M_c\cos\theta)^4}(\frac{\Omega}{a_\infty})^4 |S|^2 \beta_{11},$$

$$a_{1122} = \frac{g^2(r_o)\cos^2\theta}{2(1-M_c\cos\theta)^4}(\frac{\Omega}{a_\infty})^4 |S|^2 \beta_{12},$$

$$a_{2222} = (3/8)g^4(r_o)(\frac{\Omega}{a_\infty})^4 |S|^2 \beta_{22},$$

$$a_{2233} = (1/8)g^4(r_o)(\frac{\Omega}{a_\infty})^4 |S|^2 \beta_{23}.$$

The shielding function is

$$g^2(r,\theta) = \frac{(1-M_o\cos\theta)^2(a_\infty/a)^2 - \cos^2\theta}{(1-M_C\cos\theta)^2}.$$

It should be noted that correlation coefficients a_{ijkl} all have a Doppler-factor power of 4 in the denominator, which when multiplied by $(\Omega/a_\infty)^4$ makes a_{ijkl} proportional to the factctor k^4. Shielding coefficients β_{ij} depend on the number of turning points of $g^2(r,\theta)$ as well as location of source point r_o with respect to that of the turning point r_σ. For example, when there is only one turning point and $r_o < r_\sigma$, we have

$$\beta_{ij} \sim \exp\{-2\frac{\Omega}{a_\infty}\int_{r_o}^{r_\sigma}\sqrt{|g^2(r)|}dr\}.$$

Appendix B

For a homogeneous isotropic turbulence correlation coefficients are related to the axial components with either Gaussian or exponential spatial functions $f(\xi) = \exp(-\pi\xi^2/\ell^2)$ and $f(\xi) = \exp(-\pi\xi/\ell)$:

$$I_{2222} = I_{3333} = I_{1111},$$

$$I_{1122} = I_{1133} = I_{2233} = \frac{1}{8}I_{1111},$$

$$I_{1212} = I_{1313} = I_{2323} = \frac{7}{16}I_{1111}.$$

These relations hold for compact as well as non-compact source models.

References

[1] Bridges, J., "Measurements of Turbulent flow Field in Separable Flow Nozzles with Enhanced Mixing Devices – Test Report," NASA TM-2002-211366.

[2] Freund J. B., "Noise Source in a Low-Reynolds-Number Turbulent Jet at Mach 0.9," J. Fluid Mechanics, Vol. 438, 2001, pp. 277-305.

[3] Morris, P. J., Scheidegger, E. T., and Long, L. N., "Jet Noise Simulation for Circular Nozzles," AIAA Paper 2000-2080, June 2000.

[4] Mankbadi, R. R., and Hixon, R., "Very Large Eddy Simulations of Jet Noise," AIAA Paper 2000-2008, June 2000.

[5] Mankbadi, R. R., Hixon R., Shih, S. H., and Povinelli, L. A., "Use of Linearized Euler Equations for Supersonic Jet Noise Predictions," AIAA Journal, Vol. 36, No. 2. Feb. 1998.

[6] Seror, C., Sagaut, P., Bailly C., and Juve, D., "Subgrid-Scale Contribution to Noise Production in Decaying Isotropic Turbulence," AIAA Journal, Vol. 38, No. 10, Oct. 2000, pp. 1795-1803.

[7] Khavaran, A., "Role of Anisotropy in Turbulent Mixing Noise," AIAA Journal, Vol. 37, No. 7., 1999, pp. 832-841.

[8] Tam, C. K. W., and Auriault, L., "Jet Mixing Noise from Fine-Scale Turbulence," AIAA Journal, Vol. 37, No, 2, 1999, pp-145-153.

[9] Woodruff, S. L., Seiner, J. M., Hussani, M. Y., and Erlebacher, G., "Implementation of New Turbulence Spectra in the Lighthill Analogy Source Terms," J. Sound and Vibration, Vol. 242(2), 2001, pp. 197-214.

[10] Khavaran, A., Krejsa, E. A., and Kim, C. M., "Computation of Supersonic Jet Mixing Noise for an Axisymmetric Convergent-Divergent Nozzle," Journal of Aircraft, Vol.31, No.3, 1994, p.603-609.

[11] Hinze, J. O., *Turbulence*, 1975, New York, McGraw-Hill.

[12] Goldstein, M. E., "An Exact Form of Lilley's Equation With a Velocity Quardupole/Temperature Dipole Source Term," Journal of Fluid Mechanics, Vol. 433, 2001, pp. 231-236.

[13] Batchelor, G. K., *The Theory of Homogeneous Turbulence*, Cambridge Univ. Press, Cambridge, England, UK, 1960.

[14] Bridges, J., and Wernet, M. P., "Turbulence Measurements of Separate Flow Nozzles with Mixing Enhancement Features," AIAA Paper 2002-2484, June 2002.

[15] Tam, C. K. W., and Auriault, L., "Mean Flow Refraction Effects on Sound Radiated from Localized Sources in a Jet," Journal of Fluid Mechanics, Vol. 370, 1998, pp. 149-174.

[16] Balsa, T. F., "The Far-Field of High frequency Convected Singularities in Sheared Flows, with an Application to jet Noise Prediction," Journal of Fluid Mechanics, Vol. 74, March 1976, pp. 193-208.

[17] Chu, W. T., "Turbulence Measurements Relevant to Jet Noise," Institute for Aerospace Studies, UTIAS Report No. 119, Univ. of Toronto, Toronto, ON, Canada, Nov. 1966.

[18] Townsend, A. A., *The Structure of Turbulent Shear Flow*, Cambridge University Press, Cambridge, England, UK, 1976.

[19] Morris, J. P., and Farassat, F., "Acoustic Analogy and Alternative Theories for Jet Noise Prediction," AIAA Journal, Vol. 40, No. 7, 2002, pp. 671-680.

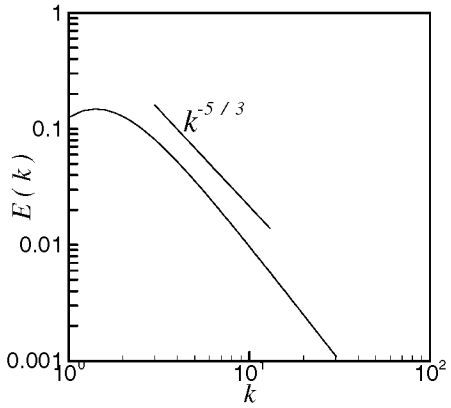

Fig. 1 Energy spectrum for the exponential function $f(\xi) = \exp(-\pi\xi / \ell)$.

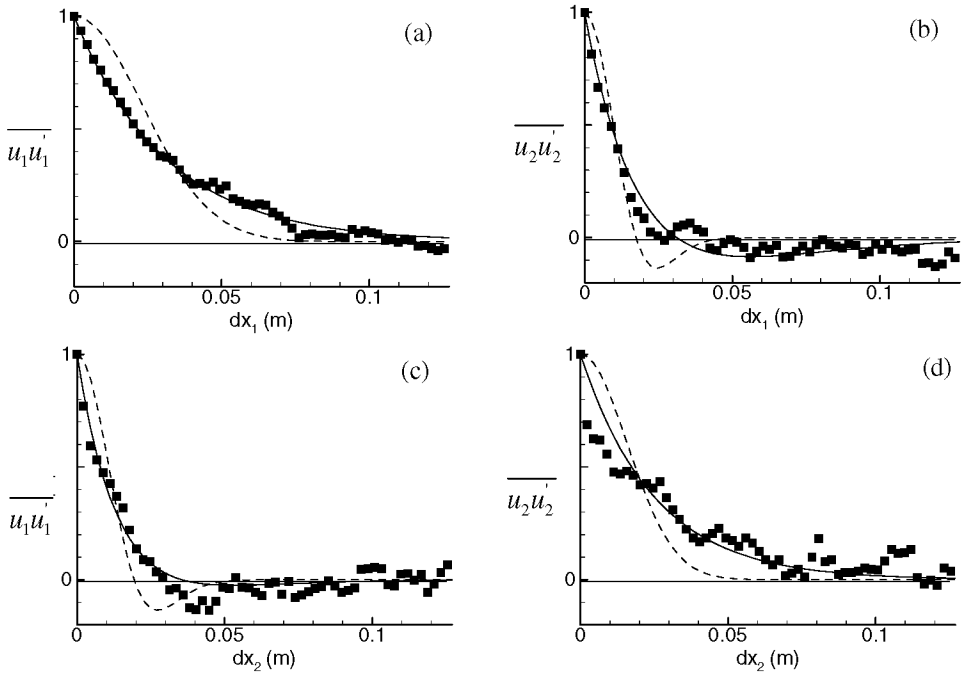

Fig. 2 Measurements of a two-point correlation $(a)\ R_{11}(\xi_1), (b)\ R_{22}(\xi_1), (c)\ R_{11}(\xi_2), (d)\ R_{22}(\xi_2)$ in a high-subsonic jet. Eq. (2.14) with Exponential function (solid line); Gaussian (dashed-line).

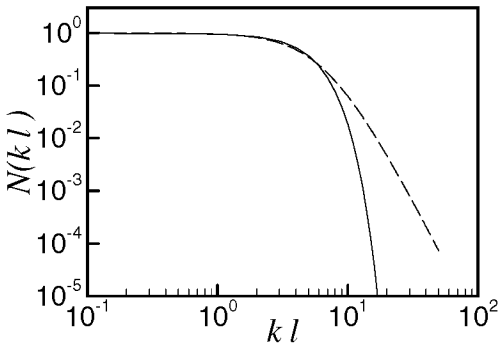

Fig. 3 **Effect of source non-compactness on the correlation coefficient with spatial function: model (a)** $f(\xi) = \exp(-\pi\xi^2 / \ell^2)$ **(solid line); model (b)** $f(\xi) = \exp(-\pi\xi / \ell)$ **(dashed-line).**

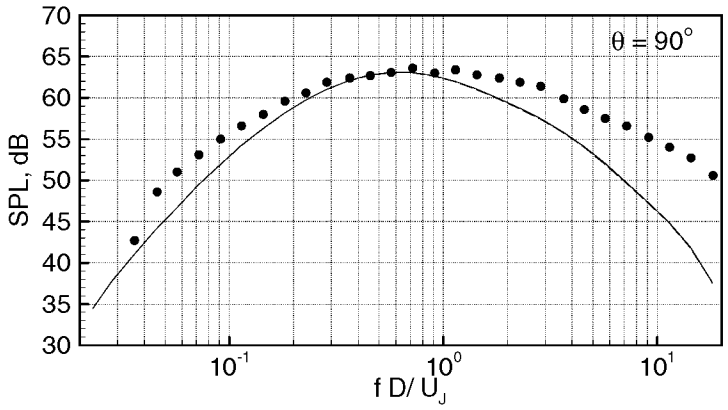

Fig. 4 **MGBK Noise spectra for Mach 0.5 cold jet. Predictions with model (a); compact source (solid line); non-compact source (dashed-line); data (symbol).**

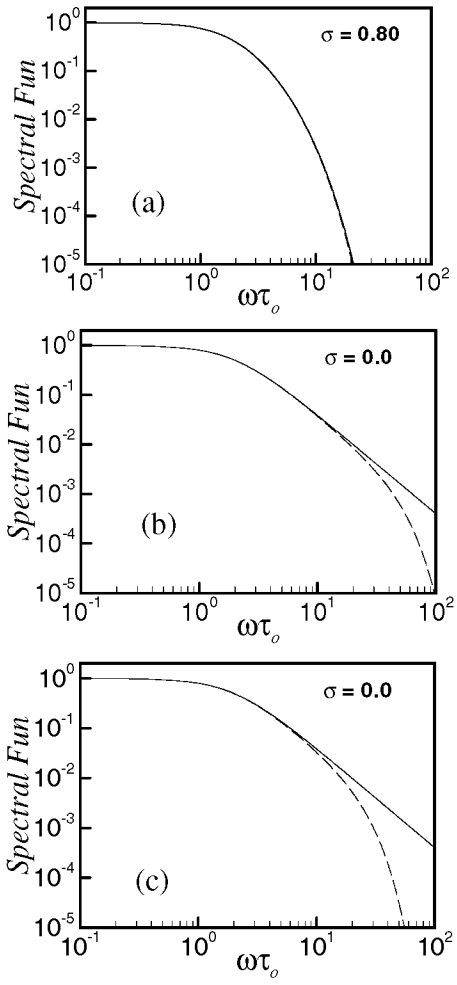

Fig. 5 **Effect of source non-compactness on spectral shape function of model (a). Compact source (solid line); non-compact source (dashed-line). (a)** $U / a_\infty = 0.50, 1.0$; **(b)** $U / a_\infty = 0.50$; **(c)** $U / a_\infty = 1.0$.

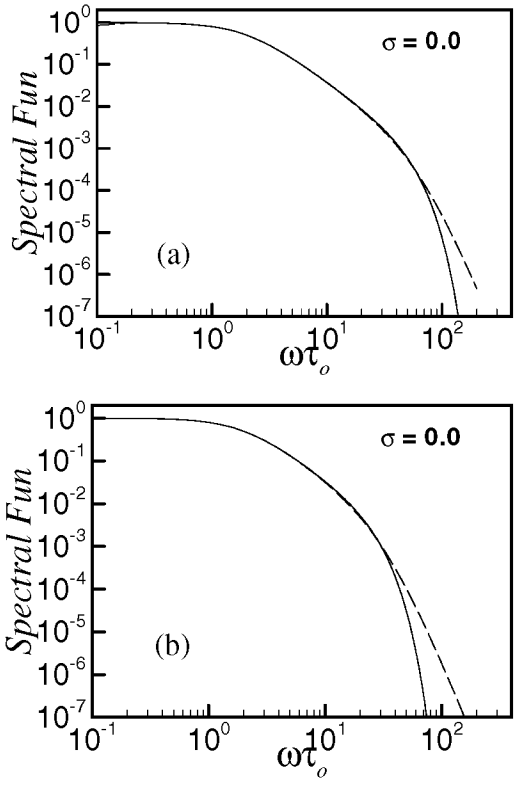

Fig. 6 **Spectral shape function for the non-compact source with**
$f(\xi) = \exp(-\pi\xi^2 / \ell^2)$ **(solid line);**
$f(\xi) = \exp(-\pi\xi / \ell)$ **(dashed-line);**
(a) $U / a_\infty = 0.50$ **, (b)** $U / a_\infty = 1.0$.

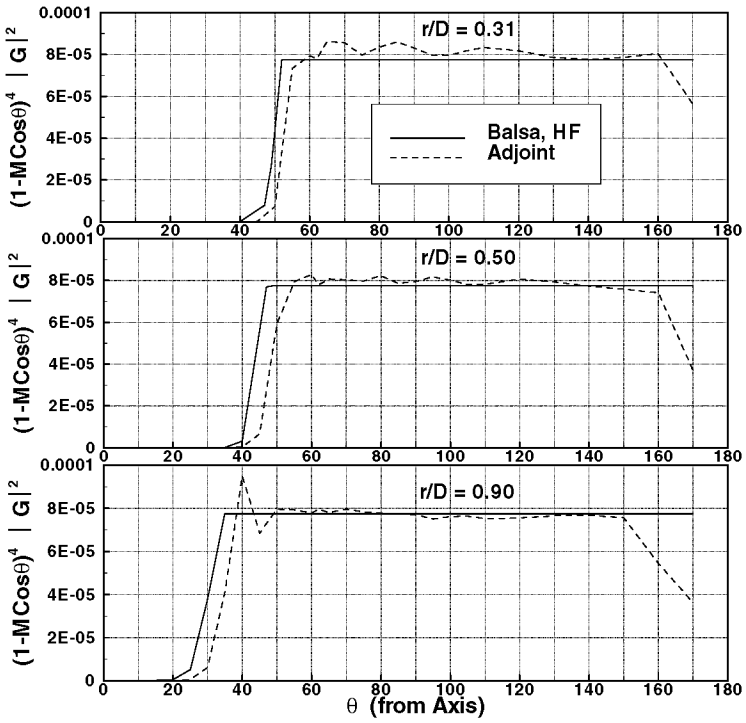

Fig. 8a **Comparison of the high frequency (HF) Green's function with the adjoint Green's function for a stationary ring source at indicated radial locations for a Mach 0.9 cold jet at St = 5.0.**

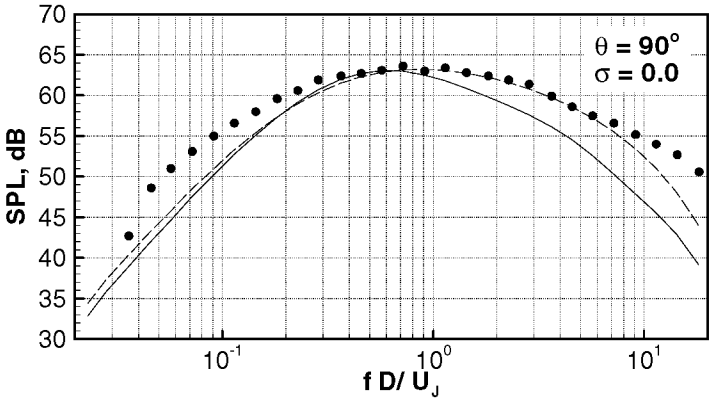

Fig. 7 **MGBK noise spectra for Mach 0.5 cold jet with a non-compact source;**
Model (a) (solid line); Model (b) (dashed-line);
data (symbol).

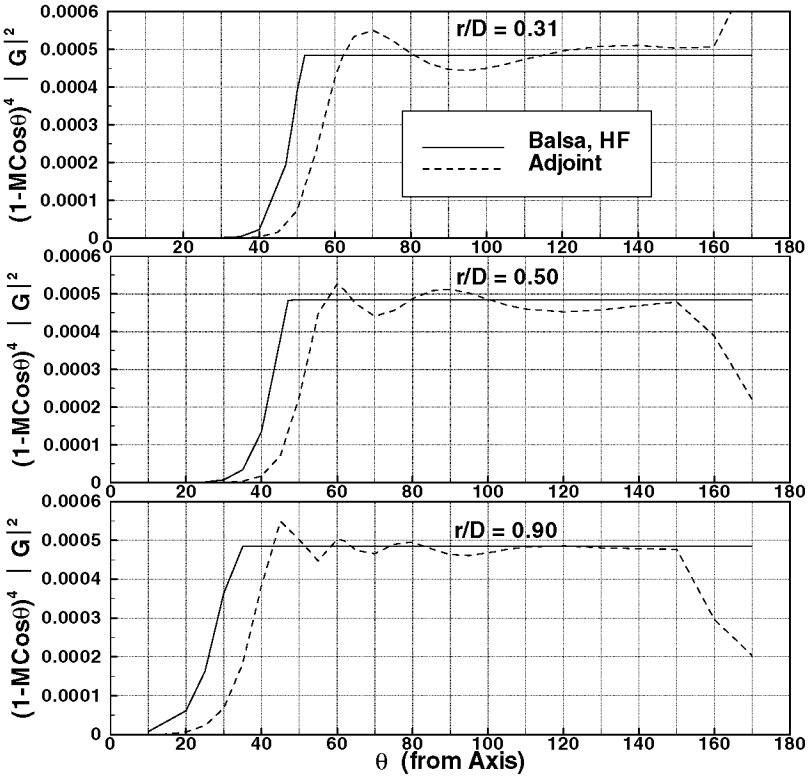

Fig. 8b Green's function comparison at St = 2.0.

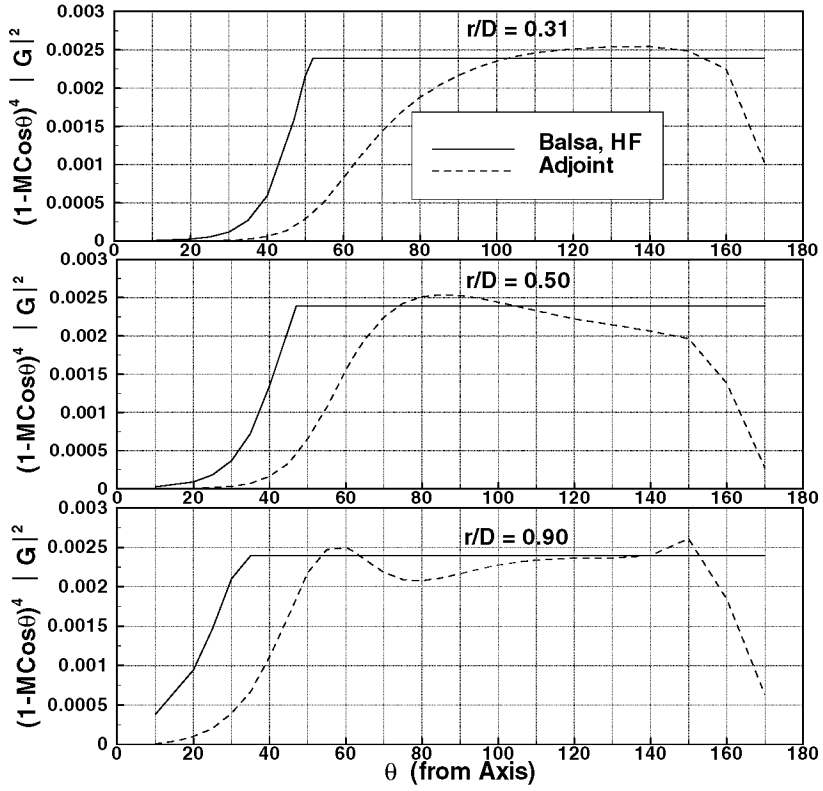

Fig. 8c Green's function comparison at St = 0.90.

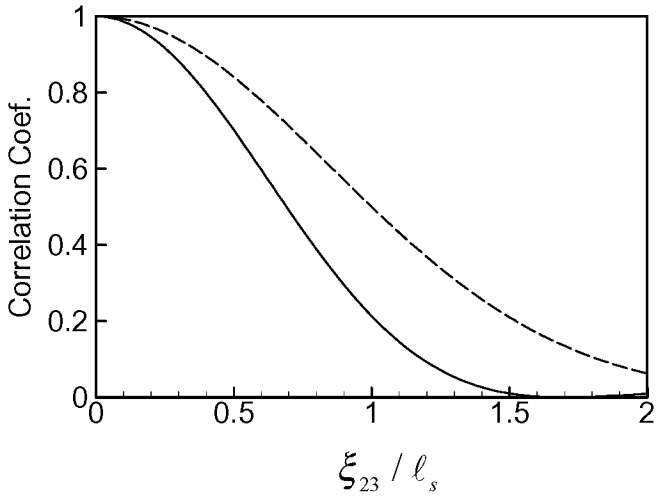

Fig. 9a Correlation coefficient $I_{1111}(\xi_{23})$: MGBK (solid-line); Tam *et al.* (dashed-line).

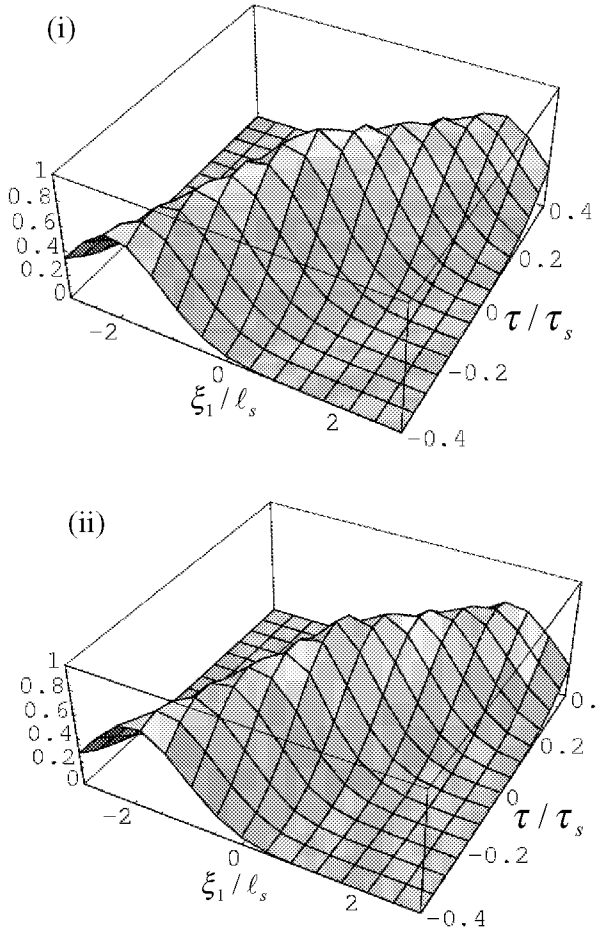

Fig. 9b Comparison of the axial cross-correlation coefficients of Tam *et al.* and MGBK. (i) Tam's model (Eq. 3.11); (ii) MGBK model (Eq. 3.12) with $\sigma = 0$.

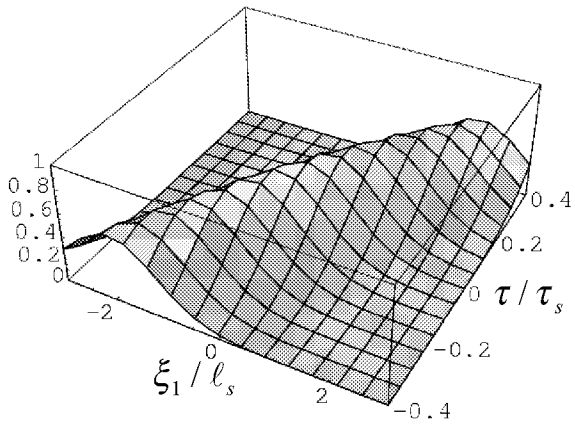

Fig. 9c MGBK cross correlation function (Eq. 3.12) with $\sigma = 0.40$.

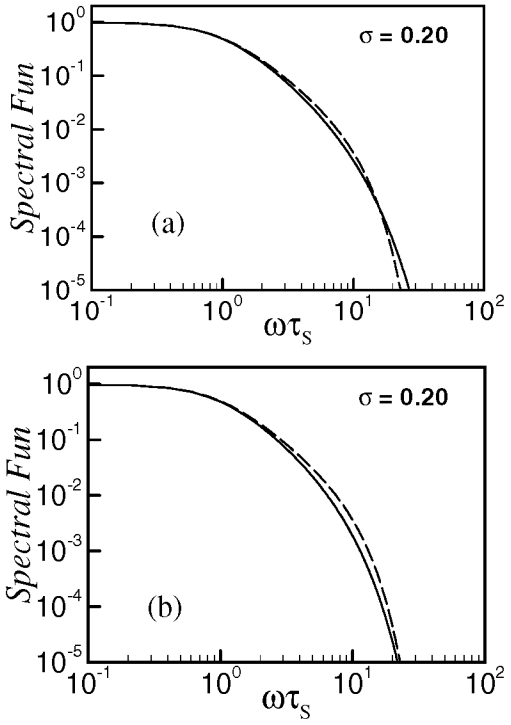

Fig. 10 **Spectral Shape function at 90°; MGBK (solid line); Tam *et al.* (dashed-line).**
(a) $U / a_\infty = 0.325$, **(b)** $U / a_\infty = 0.65$.

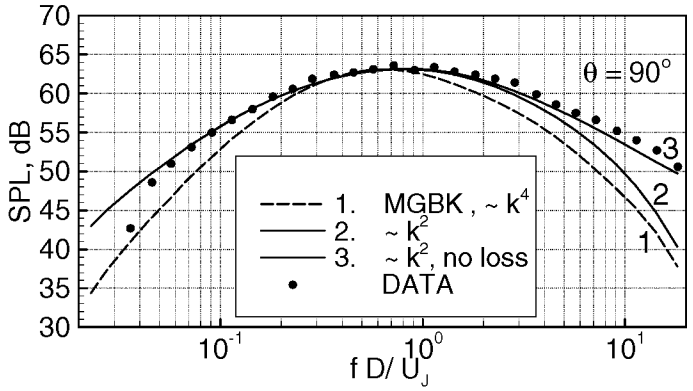

Fig. 11 **Predictions for Mach 0.5 cold jet using a spectral shape function consistent with Tam *et al.* at 90°.**

REPORT DOCUMENTATION PAGE

Form Approved
OMB No. 0704-0188

1. AGENCY USE ONLY (*Leave blank*)	2. REPORT DATE	3. REPORT TYPE AND DATES COVERED
	July 2002	Technical Memorandum

4. TITLE AND SUBTITLE

A Parametric Study of Fine-Scale Turbulence Mixing Noise

5. FUNDING NUMBERS

WU–708–90–43–00

6. AUTHOR(S)

Abbas Khavaran, James Bridges, and Jonathan B. Freund

7. PERFORMING ORGANIZATION NAME(S) AND ADDRESS(ES)

National Aeronautics and Space Administration
John H. Glenn Research Center at Lewis Field
Cleveland, Ohio 44135–3191

8. PERFORMING ORGANIZATION REPORT NUMBER

E–13428

9. SPONSORING/MONITORING AGENCY NAME(S) AND ADDRESS(ES)

National Aeronautics and Space Administration
Washington, DC 20546–0001

10. SPONSORING/MONITORING AGENCY REPORT NUMBER

NASA TM—2002-211696
AIAA–2002–2419

11. SUPPLEMENTARY NOTES

Prepared for the Eighth Aeroacoustics Conference cosponsored by the American Institute of Aeronautics and Astronautics and the Confederation of European Aerospace Societies, Breckenridge, Colorado, June 17–19, 2002. Abbas Khavaran QSS Group, Inc., Cleveland, Ohio; James Bridges, NASA Glenn Research Center; and Jonathan B. Freund, University of Illinois at Urbana-Champaign, Champaign, Illinois 61820. Responsible person, Abbas Khavaran, organization code 5940, 216–977–1120.

12a. DISTRIBUTION/AVAILABILITY STATEMENT

Unclassified - Unlimited
Subject Categories: 07 and 34 Distribution: Nonstandard

Available electronically at http://gltrs.grc.nasa.gov/GLTRS

This publication is available from the NASA Center for AeroSpace Information, 301–621–0390.

12b. DISTRIBUTION CODE

13. ABSTRACT ***(Maximum 200 words)***

The present paper is a study of aerodynamic noise spectra from model functions that describe the source. The study is motivated by the need to improve the spectral shape of the MGBK jet noise prediction methodology at high frequency. The predicted spectral shape usually appears less broadband than measurements and faster decaying at high frequency. Theoretical representation of the source is based on Lilley's equation. Numerical simulations of high-speed subsonic jets as well as some recent turbulence measurements reveal a number of interesting statistical properties of turbulence correlation functions that may have a bearing on radiated noise. These studies indicate that an exponential spatial function may be a more appropriate representation of a two-point correlation compared to its Gaussian counterpart. The effect of source non-compactness on spectral shape is discussed. It is shown that source non-compactness could well be the differentiating factor between the Gaussian and exponential model functions. In particular, the fall-off of the noise spectra at high frequency is studied and it is shown that a non-compact source with an exponential model function results in a broader spectrum and better agreement with data. An alternate source model that represents the source as a covariance of the convective derivative of fine-scale turbulence kinetic energy is also examined.

14. SUBJECT TERMS

Noise prediction; aircraft; Jet aircraft noise; Turbulence; Turbulence models; Jet mixing

15. NUMBER OF PAGES

22

16. PRICE CODE

17. SECURITY CLASSIFICATION OF REPORT	18. SECURITY CLASSIFICATION OF THIS PAGE	19. SECURITY CLASSIFICATION OF ABSTRACT	20. LIMITATION OF ABSTRACT
Unclassified	Unclassified	Unclassified	